Article:
Boiko, DL, Antonov, AV, Kuritsyn, DI et al. (4 more authors) (2017) Mid-infrared two photon absorption sensitivity of commercial detectors. Applied Physics Letters, 111 (17). ARTN 171102. ISSN 0003-6951

https://doi.org/10.1063/1.4996187

Mid-infrared two photon absorption sensitivity of commercial detectors

Cite as: Appl. Phys. Lett. **111**, 171102 (2017); https://doi.org/10.1063/1.4996187
Submitted: 14 July 2017 . Accepted: 15 October 2017 . Published Online: 26 October 2017

D. L. Boiko, A. V. Antonov, D. I. Kuritsyn, A. N. Yablonskiy, S. M. Sergeev, E. E. Orlova, and V. V. Vaks

Mid-infrared two photon absorption sensitivity of commercial detectors

D. L. Boiko,[1,a)] A. V. Antonov,[2] D. I. Kuritsyn,[2] A. N. Yablonskiy,[2] S. M. Sergeev,[2] E. E. Orlova,[2,b)] and V. V. Vaks[2]
[1]*Centre Suisse d'Electronique et de Microtechnique SA (CSEM), CH-2002 Neuchâtel, Switzerland*
[2]*Institute for Physics of microstructures, 603087 Nizhnij Novgorod, Russia*

(Received 14 July 2017; accepted 15 October 2017; published online 26 October 2017)

We report on broad-band two-photon absorption (TPA) in several commercially available MIR inter-band bulk semiconductor photodetectors with the spectral cutoff in the range of 4.5–6 μm. The highest TPA responsivity of 2×10^{-5} A·mm^2/W^2 is measured for a nitrogen-cooled InSb photovoltaic detector. Its performance as a two-photon detector is validated by measuring the second-order interferometric autocorrelation function of a multimode quantum cascade laser emitting at the wavelength of 8 μm. *Published by AIP Publishing*. https://doi.org/10.1063/1.4996187

Strong vibrational transitions of molecules in the mid-infrared (MIR) spectral region as well as the two atmospheric transmission windows at 3–5 μm and 8–13 μm render this spectral range highly attractive for applications in spectroscopy, material processing, chemical and biomolecular sensing, security, and gas analysis. Several important applications, such as time-resolved spectroscopy, remote sensing, and high speed optical communication, have stimulated the development of MIR lasers producing short radiation pulses and MIR detectors.

Continuously operating quantum cascade lasers (QCLs) have reached the industrial maturity level and have become the primary spectroscopic tool for MIR photonics due to their design flexibility, high gain, and tunability.[1] The broad-band gain in such lasers potentially admits ultra-fast pulse production regimes. However, unambiguous demonstration of QCLs capable of producing short MIR optical pulses remains a challenge due to the picosecond carrier relaxation time and their relatively low average output powers.[2–7]

The measurement of the second-order autocorrelation function is crucial for characterization of ultra-short optical pulses. For MIR QCLs producing relatively low output power, two-photon GaAs/InGaAs quantum well infrared photodetectors (2P-QWIP) have been favored.[8,9] They provide an adequate two-photon absorption (TPA) sensitivity, whereas the second harmonic conversion efficiency of nonlinear crystals in the MIR range is too low for applications with QCLs.[2] However, 2P-QWIPs have a narrow spectral range (below 300 nm), and thus, a dedicated epitaxy run is usually needed for a specific QCL sample. At the same time, photovoltaic and photoconductive detectors based on inter-band TPA in narrow-gap InSb and InAsSbP materials can provide a much broader TPA spectral range, and these detectors are readily available. However, the TPA regime of inter-band detectors has only been used before for autocorrelation measurements in the visible range[10,11] or for mid-infrared radiation pulses with the power much higher than that of MIR QCLs.[12]

In this letter, we report on the MIR TPA response measured using several commercial detectors with the single-photon absorption (SPA) cut-off in the range of 4.5–6 μm. We demonstrate the use of such detectors for the second-order interferometric autocorrelation measurements in low-power QCL operating in the multimode regime[2] and emitting at a wavelength of 8 μm.

The MIR detectors used in this study (Table I) include a photovoltaic InSb detector (referenced as #1), a photoconductive InSb detector (#2), an InAsSbP p-i-n photodiode (#3), and a photoconductive InAsSbP detector (#4). All these detectors have the sensitivity cut-off at a wavelength of around 4.5–6 μm. Their linear response characteristics at peak sensitivity wavelengths and the noise figures are reproduced from the manufacturer data sheets except for detector #2, which is a home-built detector. The results obtained in this study are shown in the second portion of Table I devoted to the TPA responsivity at the wavelength of 8 μm.

Detector #1 is packaged in a metal dewar for cryogenic cooling. It was initially equipped with a sapphire window which does not transmit photons with energies below the detector cut-off. To perform the TPA measurements, we have replaced it with a ZnSe window transparent at 7–8 μm. For the same purpose, we have removed the encapsulation cover and the Si window from detector #4. Detector #3 is equipped with an additional parabolic reflector with the detector chip located at the center of the reflector to improve the detectivity for wide parallel beams. Although the measurements were performed using focused beams with the diameters well below the reflector size, we cannot exclude that the parabolic reflector might have some influence on the measured TPA characteristics of this detector.

The measured detector signals in the TPA regime (see Figs. 2 and 3 discussed below) demonstrate a combined effect of the linear and quadratic responses and exhibit saturation[13,14] at power levels well below the absorption saturation.[15,16] Such a behavior of TPA detectors is well reported in the literature. In order to simplify the comparison of the TPA detectors from Table I, we remind several important points. The low saturation threshold in bulk TPA detectors can be attributed to the field screening that yields a linear saturation of the output photocurrent.[13,14]

[a)]Author to whom correspondence should be addressed: dmitri.boiko@csem.ch.
[b)]Present address: Pollard Institute, School of Electrical and Electronics Engineering, University of Leeds, Leeds LS2 9JT, United Kingdom.

TABLE I. Parameters of detectors used in this study.

	Detector #1 Photovoltaic InSb detector IS-2.0 InfraRed Associates	Detector #2 InSb photoresistor (home-built)	Detector #3 InAsSbP–pin photodiode PD48-03	Detector #4 InAsSbP –photoresistor PR-43
Detector area, A_D	$\pi \cdot 1^2$ mm^2	5×5 mm^2	$\pi \cdot 0.15^2$ mm^2	2×2 mm^2
Cut-off wavelength	5.5 μm	5.9 μm	4.9 μm	4.5 μm
Linear response characteristics at $\lambda \sim 4.5$–5 μm				
Peak sensitivity wavelength	5.3 μm	5.5 μm	4.5 μm	3.8 μm
Peak responsivity K_1	3 A/W	0.065 A/W	0.91 A/W	0.02 A/W
Current noise PSD, i_n	3.3×10^{-12} A/Hz$^{1/2}$	73×10^{-12} A/Hz$^{1/2}$	0.97×10^{-12} A/Hz$^{1/2}$	8×10^{-12} A/Hz$^{1/2}$
BW	2 MHz	35 kHz	17 MHz	35 kHz
TPA characteristics at $\lambda = 8$ μm				
SPA responsivity k_1	1×10^{-6} A/W	9×10^{-5} A/W	4×10^{-6} A/W	1.2×10^{-7} A/W
TPA responsivity k_2	2.0×10^{-5} A·mm^2/W^2	9.2×10^{-6} A·mm^2/W^2	9.3×10^{-8} A·mm^2/W^2	1.1×10^{-8} A·mm^2/W^2
CW saturating beam size parameter w_{sat}	9.9 mm	0.68 mm	0.46 mm	0.32 mm
Saturation current I_{sat} (power I_{sat}/k_1)	30 μA (30 W)	2.6 mA (29 W)	0.22 mA (56 W)	0.84 μA (7.2W)
SNR performance figure k_2/i_n	6.1×10^6 mm^2 Hz$^{1/2}$/W^2	1.3×10^5 mm^2 Hz$^{1/2}$/W^2	9.6×10^4 mm^2 Hz$^{1/2}$/W^2	1.3×10^3 mm^{2}Hz$^{1/2}$/W^2
Operation temperature	77 K	77 K	300 K	300 K

$$I/I_{sat} = (RP + SP^2)/(RP + SP^2 + I_{sat}), \tag{1}$$

where P is the incident power, I_{sat} is the saturation current, and R (units A/W) and S (units A/W^2) are the linear and quadratic contributions to the output photocurrent. (The responsivities of photoconductive detectors at a fixed bias and those of the photovoltaic detectors are characterized in the same way[17]).

The linear SPA response and saturation effects in (1) limit the dynamic range of the TPA detector. However, it can be easily tailored by changing the illumination spot size at the detector. Indeed, assuming that the detector is illuminated with a Gaussian beam of diameter $2w$ (at e^{-2} intensity level), which is smaller than the detector sensitive region, the apparent linear and quadratic responsivities of the TPA detector can be expressed as

$$R = k_1 G_{T1}, \quad S = k_2 G_{T2}/\pi w^2, \tag{2}$$

where the factors G_{T1} and G_{T2} account for the temporal response of the detector. (These factors are equal to unity for CW illumination.) The coefficients k_1 (units A/W) and k_2 (units Acm^2/W^2) shown in Table I are independent of the illumination conditions and characterize the intrinsic SPA and TPA responsivities of the detector. (The linear SPA responsivity k_1 for photon energies below the sensitivity cut-off is of 5–6 orders of magnitude lower than that at the sensitivity peak.)

For what follows, it is convenient to normalize the incident power to its saturation level in the linear SPA response regime and introduce a variable $\zeta = PR/I_{sat}$. The range of incident powers ζ in which a quadratic TPA response can be observed at the detector output follows from Eq. (1):

$$\rho^{-2} < \xi < \frac{\sqrt{1 + 4\rho^2} - 1}{2\rho^2}, \tag{3}$$

where we have introduced a parameter ρ that characterizes the dynamic range of the detector [see Eq. (5)] and combines all parameters from Eq. (1):

$$\rho = \frac{\sqrt{SI_{sat}}}{R} = \frac{\sqrt{G_{T2}}}{G_{T1}} \frac{\sqrt{2} w_{sat}}{w}. \tag{4}$$

The TPA response at the detector output is possible if $\rho > \sqrt{2}$. This parameter scales inversely with the beam size w. For CW illumination conditions ($G_{T1}^{(CW)} = G_{T2}^{(CW)} = 1$), $w_{sat} = \sqrt{k_2 I_{sat}/2\pi}/k_1$ is the maximum beam size parameter for which the TPA response can be observed prior to the detector saturation. The extracted w_{sat} values for our detectors are shown in Table I. Tighter beam focusing not only leads to a reduction of the minimum power required to observe the TPA response [left hand side of Eq. (3)] but also reduces the power at which the detector saturates [right hand side of Eq. (3)]. However, the overall dynamic range of the TPA detector increases:

$$P_{max}/P_{min} \approx \rho. \tag{5}$$

This approximation is fairly good when $\rho \gg 1$.

An example of the responsivity curve in a bulk TPA detector (1) operating at $\rho = 10^3$ is depicted in Fig. 1(a) (blue curve). The region without gray shadow highlights the 30 dB dynamic range of TPA responses (5). The black dashed curve is a guide to the eye, indicating the characteristic slope $I \propto P^2$. The response of the bulk TPA detector (1) follows this quadratic curve very well. For comparison, we also plot the response of 2P-QWIP (green curve) calculated for the same dynamic range of TPA responses ($\rho = 10^3$) and using the model from Refs. 13 and 14

$$I = (RP + SP^2) W\{I_{sat}/(RP + SP^2)\}, \tag{6}$$

where W(z) is the Lambert function. Because the 2P-QWIP exhibits logarithmic saturation, the slope of the response curve is lower than $I \propto P^2$. As a consequence, the second-order autocorrelation function measured with such 2P-QWIP would require a correction[13] if a tighter beam focusing or pulse compression cannot be achieved in the experimental setup.

In Fig. 1(b), with the increase in the dynamic range of the bulk TPA detector (by tighter beam focusing), the entire

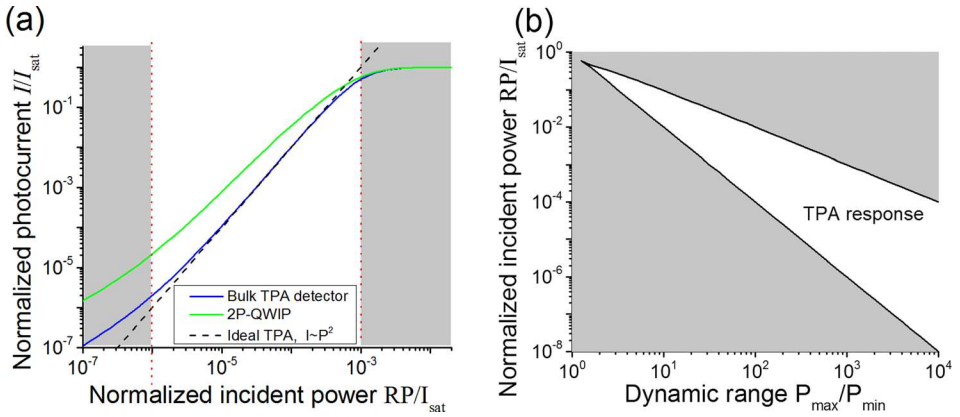

FIG. 1. (a) Modelled responsivity curves for the bulk TPA detector (blue curve) and 2P-QWIP (green curve) for the dynamic range parameter of $\rho=10^3$. The black dashed curve indicates the characteristic slope $I \propto P^2$. (b) Relationship between the dynamic range (5) and incident power (3) in the bulk TPA detector or 2P-QWIP. In (a) and (b), the TPA response is observed in the opened-up region without gray shadow.

TPA response range shifts to lower powers until the photocurrent reaches the level of noise [not shown in the figure]. The signal to noise ratio (SNR) in different TPA detectors in Table I can be compared examining the ratio of k_2/i_n, with i_n^2 being the power spectral density of the detector current noise. Above the noise limit, the dynamic range and the sensitivity of the TPA detector can be tailored by focusing the incident beam (4) such that $\rho = \sqrt{I_{sat}/RP_{\min}}$ [see the left-hand side of Eq. (1)].

We have tested the TPA responsivity of the detectors from Table I under both quasi-CW and pulsed illumination conditions. For pulsed illumination, an optical parametric oscillator (OPO InfraTune, Solar Laser Systems) was used. It is tunable in the range of 7–9 μm and emits MIR pulses of $\tau_{FWHM}\sim$10 ns width and repetition rate $F_{rep}=$10 Hz. Additional spectral filters were introduced in the optical setup to suppress the residue pump and OPO signal beams. The linearly polarized idler beam was attenuated with an adjustable broadband polarizer (CVI Laser) and focused at the detector using one of the ZnSe lenses of 50, 30, 20, or 15 mm focal length. The output of the detector was amplified using a trans-impedance amplifier (SR570, Stanford Research Systems) and captured on a digitizing oscilloscope (WaveSurfer 432, LeCroy). All the detectors listed in Table I have small bandwidths and provide only an integrated response defined by a convolution of the detector impulse function and an excitation pulse of 10 ns. Because the illumination pulse train had a low duty cycle, it was possible to register the peak photocurrent for individual illumination pulses, yielding

$$G_{T1} = BW/F_{rep}, \quad G_{T2} = \sqrt{2\ln 2/\pi}BW/F_{rep}^2\tau_{FWHM}, \quad (7)$$

where BW is the detector bandwidth, τ_{FWHM} is the FWHM of the optical pulse (Gaussian pulse shape model), and F_{rep} is the pulse repetition frequency. These expressions are valid for $F_{rep} \ll BW \ll 1/\tau_{FWHM}$. For example, for a detector bandwidth of 35 kHz (2 MHz), the factor $\sqrt{G_{T2}}/G_{T1}$ in Eq. (4) provides a 16 dB (7 dB) enhancement in the TPA dynamic range and a 33 dB (15 dB) improvement in the TPA sensitivity [see Fig. 1(b)].

In Fig. 2, we plot the measured detector responses as a function of the incident power. The photovoltaic detector (#3) was tested unbiased, while 3 mV bias was applied to photoconductive detectors #2 and 4. (Detector #1 is not shown because it has much higher sensitivity and was saturated.) By adjusting the focusing lens, we obtained the TPA response in all the detectors despite the fact that their saturation currents differ by 3 orders of magnitude. The TPA responsivities k_2 of the detectors have been obtained by numerically fitting the measured curves to the model in Eq. (1). An example of the model fit is indicated for detector #4 (right axis). The linear response k_1 coefficient was defined either from the fit or from the measurements with a CW operating quantum cascade laser (QCL) as discussed below. To confirm the broad spectral range of TPA sensitivity of bulk detectors, we measured the response curves of detector #2 at wavelengths of 7 μm and 8 μm and find them to be very similar to each other.

Next, we have measured the response curves of the detectors under illumination from a continuously operating multimode QCL (Alpes Lasers) emitting at 8 μm. The output beam of QCL was collimated and refocused at a detector by a system of two ZnSe lenses with focal distances of 4.7 and 20 mm (or with a pair of 4.7 and 15 mm). A chopper was installed in front of the refocusing lens to reduce the detector heating, transforming the CW illumination into a square pulse train with the frequency of 70 Hz and the duty cycle of 1:12. The temporal width of illumination pulses largely exceeds the detector response time, and thus, the detector operates in the quasi-CW illumination regime. The output of the detector was amplified using a trans-impedance amplifier (SR570, Stanford Research Systems) followed by a lock-in

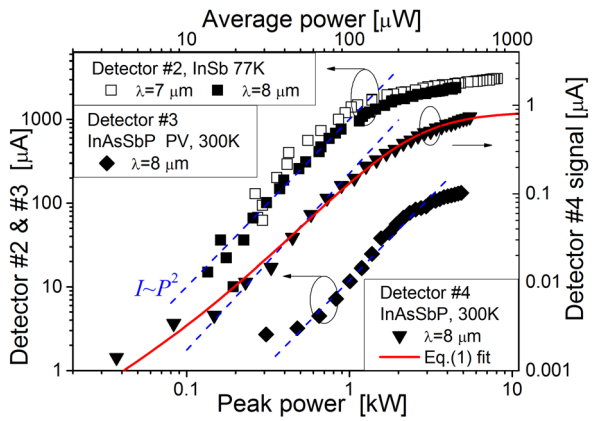

FIG. 2. Measured detector responses under pulsed illumination by OPO at wavelengths of 7 μm and 8 μm. Left axis: detector #2 cooled to 77 K and detector #3 at room temperature; Right axis: detector #4 at room temperature. The red curve shows the numerical fit with model (1). The blue dashed lines indicate the slope $I \propto P^2$.

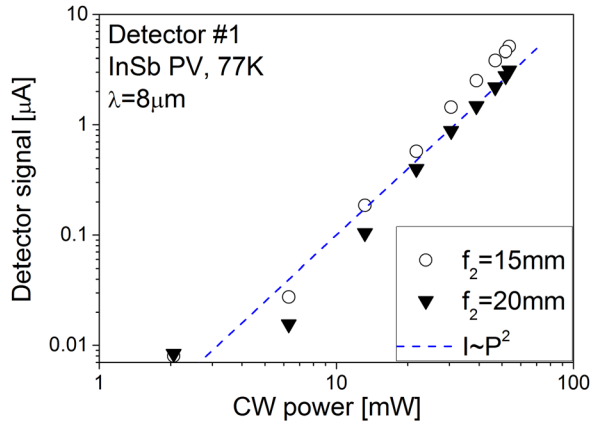

FIG. 3. Measured TPA response of detector #1 under quasi-CW illumination from a QCL with two different lenses of 15 and 20 mm focal lengths. The blue dashed line indicates the slope due to the detector response in the TPA regime.

amplifier (SR830). We recorded the value of the steady-state photocurrent at the end of each optical pulse.

Without the sensitivity improvement by the temporal factors ($G_{T1} = G_{T2} = 1$), we observed the TPA response only in photovoltaic InSb detector #1 (Fig. 3), while other detectors exhibited a linear response (not shown in the figure). In fact, all the detectors have the saturating power I_{sat}/k_1 in the range of tens of Watts (see Table. I). In order to reach TPA sensitivity at the $P_{min}\sim 1$ mW level, which is 4 orders of magnitude below the saturation, the incident beam should be focused to reach $\rho \sim 100$ [see Eq. (3)]. However, all the detectors except for detector #1 have the saturating beam size parameter $w_{sat} \sim 0.5$ mm (see Table I). For these detectors, the focused beam spot should be on the order of one wavelength [$\sqrt{2}w_{sat}/\rho \sim 7\ \mu$m, see Eq. (4)], which is not feasible. A different situation occurs in the case of detector #1 where $w_{sat} \sim 10$ mm and the beam should be focused just into a 160 μm diameter spot. Indeed, we have measured a quadratic response in detector #1 (Fig. 3) when we placed the 15 mm or 20 mm focusing lens in front of the detector. The simultaneous numerical fit of these data provides the TPA responsivity k_2, saturating beam size parameter w_{sat} (see Table I), and the beam spot diameters of $2w \sim 120$ and 160 μm for the two lenses (these values match the focal distance ratio).

Analyzing the data in Table I, we conclude that detector #1 is the most promising TPA detector as it shows the largest saturating beam size parameter w_{sat}. In order to validate its performance in practical applications, we have measured interferometric auto-correlation (IAC) traces using a variable-delay Michelson interferometer of a commercial Fourier transform infra-red (FTIR) spectrometer Vertex 80 operated in a step scan mode. We use a single-section Fabry-Pérot cavity QCL operating in a multimode regime[2,6] as an illumination source. The output QCL beam was collimated by the f = 4.7 mm ZnSe lens and fed to the spectrometer entrance port using another ZnSe lens (f = 50 m). The autocorrelation traces are acquired using either a linear-response MCT detector (a reference) or the TPA photovoltaic InSb detector. Under conditions approaching Risken-Nummedal-Graham-Haken (RNGH) instability,[3,4] our QCL shows splitting of the optical spectrum in two nearly symmetric sidebands. An example of the optical spectrum at the pump current 1.25 times above the lasing threshold is shown in Fig. 4(a).

The 1st-order interferometric pattern measured with the linear MCT detector [Fig. 4(b)] reveals a short coherence time of 0.66 ps. As expected, the peak to background ratio of this field interference pattern is 2:1. However, when the linear response detector was replaced by the TPA detector, the peak to background ratio increased to 8:3. This contrast value is close to the one observed in Ref. 2 using 2P-QWIP and evidences for a noisy CW intensity waveform of QCL.[18] Such a behavior can possibly be attributed to the generation of a quasiperiodic chaotic pulse train (an example can be found in Refs. 3 and 4). Further investigation of QCL dynamic behavior is left for another study. Most importantly, this result validates the application of detector #1 for measurements of the 2nd order IAC functions in QCLs.

In summary, we have shown that bulk MIR InSb photovoltaic detectors can efficiently operate in the TPA regime at 10 mW CW power, offering TPA sensitivity in a broad spectral range around 8 μm. Unlike 2P-QWIPs showing gradual (logarithmic) saturation, bulk TPA detectors exhibit an

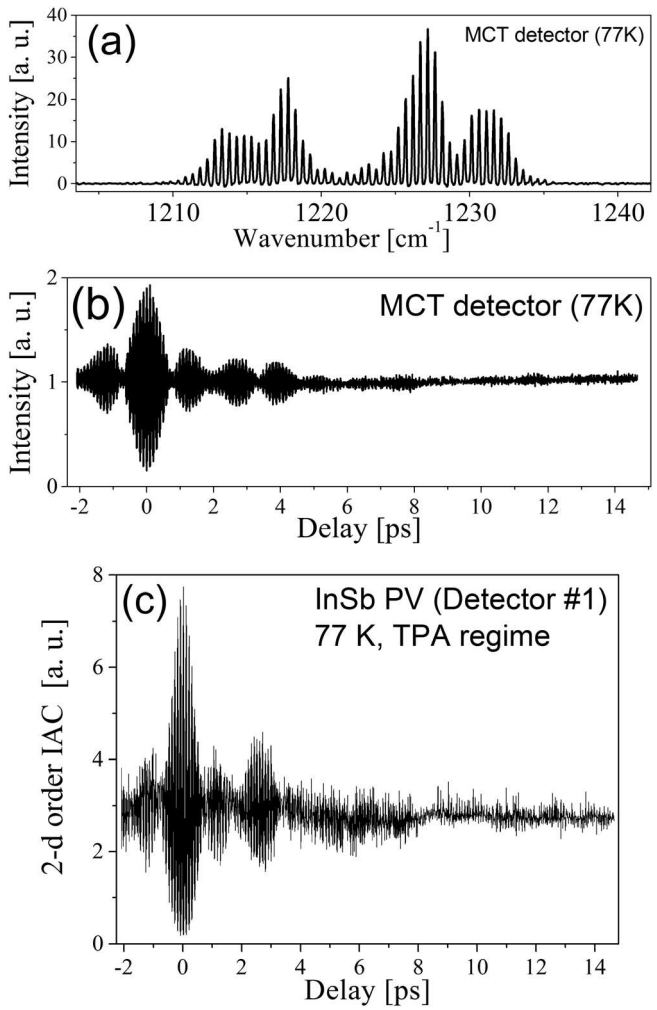

FIG. 4. Spectral (a) and interferometric traces of radiation from multi-mode QCL in CV operation at a pump current of 0.75 A and a temperature of −25 °C registered with a linear MCT detector (b) and TPA InSb detector (c). The interferograms are taken in the step-scan mode.

abrupt linear saturation, rendering their response curves steeper and showing true quadratic slopes.[13]

The authors would like to thank S. Kundermann for contribution in setup design and part procurement. D.B. is grateful to Valentin Mitev for valuable discussions. This research was supported by the Swiss National Science Foundation (SNF) Project FASTIQ (Ref. No. IZ73Z0_152761), COST action BM1205, and the Canton of Neuchâtel. QCL samples used in this research have been provided by Alpes Lasers.

[1]J. Faist, *Quantum cascade Lasers* (Oxford University Press, 2013).
[2]A. Gordon, C. Y. Wang, L. Diehl, F. X. Kärtner, A. Belyanin, D. Bour, S. Corzine, G. Höfler, H. C. Liu, H. Schneider, T. Maier, M. Troccoli, J. Faist, and F. Capasso, Phys. Rev. A **77**, 053804 (2008).
[3]N. Vukovic, J. Radovanovic, V. Milanovic, and D. L. Boiko, IEEE J. Sel. Top. Quantum Electron **23**, 1200616 (2017).
[4]N. Vukovic, J. Radovanovic, V. Milanovic, and D. L. Boiko, Opt. Express **24**, 26911 (2016).
[5]C. Y. Wang, L. Kuznetsova, V. M. Gkortsas, L. Diehl, F. X. Kärtner, M. A. Belkin, A. Belyanin, X. Li, D. Ham, H. Schneider, P. Grant, C. Y. Song, S. Haffouz, Z. R. Wasilewski, H. C. Liu, and F. Capasso, Opt. Express **17**, 12929 (2009).
[6]T. S. Mansuripur, C. Vernet, P. Chevalier, G. Aoust, B. Schwarz, F. Xie, C. Caneau, K. Lascola, C. Zah, D. P. Caffey, T. Day, L. J. Missaggia, M. K. Connors, C. A. Wang, A. Belyanin, and F. Capasso, Phys. Rev. A **94**, 063807 (2016).
[7]A. Hugi, G. Villares, S. Blaser, H. C. Liu, and J. Faist, Nature **492**, 229 (2012).
[8]H. Schneider, H. C. Liu, S. Winnerl, O. Drachenko, M. Helm, and J. Faist, Appl. Phys. Lett. **93**, 101114 (2008).
[9]H. Schneider, H. C. Liu, S. Winnerl, C. Y. Song, O. Drachenko, M. Walther, J. Faist, and M. Helm, Infrared Phys. Technol. **52**, 419 (2009).
[10]T. Feurer, A. Glass, and R. Sauerbrey, Appl. Phys. B **65**, 295 (1997).
[11]W. Rudolph, M. Sheik-Bahae, A. Bernstein, and L. F. Lester, Opt. Lett. **22**, 313 (1997).
[12]J. Burghoorn, V. F. Anderegg, T. O. Klaasen, W. T. Wenckebach, R. J. Bakker, A. F. G. van der Meer, D. Oepts, and P. W. van Amersfoort, Appl. Phys. Lett. **61**, 2320 (1992).
[13]H. Schneider, O. Drachenko, S. Winnerl, M. Helm, T. Maier, and M. Walther, Infrared Phys. Technol. **50**, 95 (2007).
[14]H. Schneider, O. Drachenko, S. Winnerl, M. Helm, and M. Walther, Appl. Phys. Lett. **89**, 133508 (2006).
[15]A. Miller, A. Johnston, J. Dempseq, J. Smith, C. R. Pidgeon, and G. D. Holah, J. Phys. C: Solid State Phys. **12**, 4839 (1979).
[16]J. Y. Duboz, E. Costard, J. Nagle, J. M. Berset, and J. M. Ortega, J. Appl. Phys. **78**, 1224 (1995).
[17]B. E. A. Saleh and M. C. Teich, *Fundamentals of Photonics* (John Wiley & Sons, Inc., 1991).
[18]J.-C. Diels and W. Rudolph, *Ultrashort Laser Pulse Phenomena*, 2nd ed. (Academic Press, 2006).